

# Regularization of functional connectomes and its impact on geodesic distance and fingerprinting

Kausar Abbas<sup>12</sup>, Mintao Liu<sup>12</sup>, Manasij Venkatesh<sup>3</sup>, Enrico Amico<sup>45</sup>, Jaroslaw Harezlak<sup>6</sup>, Alan David Kaplan<sup>7</sup>, Mario Ventresca<sup>2</sup>, Luiz Pessoa<sup>38</sup>, Joaquín Goñi<sup>129\*</sup>

<sup>1</sup> Purdue Institute for Integrative Neuroscience, Purdue University, West Lafayette, IN, USA

<sup>2</sup> School of Industrial Engineering, Purdue University, West Lafayette, IN, USA

<sup>3</sup> Department of Electrical and Computer Engineering, University of Maryland, College Park, MD, USA

<sup>4</sup> Institute of Bioengineering. Center for Neuroprosthetics. École Polytechnique Fédérale de Lausanne, Lausanne, Switzerland.

<sup>5</sup> Department of Radiology and Medical Informatics, University of Geneva (UNIGE), Geneva, Switzerland

<sup>6</sup> Department of Epidemiology and Biostatistics, Indiana University, IN, USA

<sup>7</sup> Lawrence Livermore National Laboratory. Livermore, CA, USA

<sup>8</sup> Department of Psychology and Maryland Neuroimaging Center, University of Maryland, College Park, MD, USA

<sup>9</sup> Weldon School of Biomedical Engineering, Purdue University, West Lafayette, IN, USA

\* corresponding author: jgonicor@purdue.edu

## Abstract

Functional connectomes, which are symmetric correlation matrices, have been used to study changes in brain organization with aging, cognitive abilities and across a wide range of brain disorders. They have also been shown to provide a reproducible individual fingerprint, which has opened the possibility of personalized medicine for neuro/psychiatric disorders. Thus, an accurate way to compare functional connectomes is essential. Canonically, functional connectomes are compared using Pearson's correlation coefficient of the entire functional connectivity profiles. Recently, Venkatesh and colleagues proposed the use of *geodesic distance* as a more accurate way of comparing functional connectomes, one which reflects the underlying non-Euclidean geometry of the data. They evaluated their approach in the context of participant identification (or *fingerprinting*) and showed that it leads to higher identification rates for all functional MRI conditions assessed. Computing geodesic distance requires that the functional connectivity matrices being compared are invertible (or positive-definite). As this requirement depends on the fMRI scanning length and the parcellation used, it is not always attainable. Hence Venkatesh and colleagues employed a simple regularization procedure to ensure that the matrices were invertible. In the present technical note, we show that regularization is not only crucial for making the functional connectomes invertible, but also that an optimal magnitude of regularization can lead to systematically higher identification rates. We also show that this optimal value of regularization is highly dataset-dependent, and varies as a function of condition, parcellation, and the number of frames used to compute the functional connectomes.

## 1. Introduction

Brain activity can be estimated, indirectly, by measuring the Blood Oxygenation Level Dependent (BOLD) signal using magnetic resonance imaging (MRI)<sup>1-5</sup>. This is the standard technique to generate brain images in functional MRI (fMRI) studies. Functional connectivity between two

distinct brain regions is then defined as the statistical dependence between the corresponding BOLD signals, canonically estimated with Pearson's correlation coefficient<sup>6,7</sup>. A whole-brain functional connectivity pattern can be represented as a full symmetric correlation matrix denominated Functional Connectome (FC). FCs have been used to study the changes in brain connectivity with aging<sup>8</sup>, cognitive abilities<sup>9,10</sup> and across a wide range of brain disorders<sup>11-13</sup>. Recently, it has also been shown that FCs have a recurrent and reproducible individual fingerprint<sup>14-21</sup>, which has opened the possibility of personalized medicine for neuro/psychiatric disorders<sup>18</sup>, aided by improved acquisition parameters and the availability of large datasets with open data policy<sup>22-28</sup>.

A clinically useful individual-level biomarker must have high inter-individual differentiability which in turn requires an accurate way of comparing individual FCs. FCs are compared traditionally by computing the Pearson correlation between their upper-triangular vectorized versions<sup>14,21,29</sup>. This approach enables us to assess to what extent it is possible to identify a participant from a large population of participants, a process known as fingerprinting or participant identification<sup>14</sup>.

Very recently, Venkatesh et al<sup>15</sup> introduced a geometry-aware approach to establish a more accurate way of measuring distance between any two FCs. FCs computed using Pearson's correlation coefficient between BOLD signals of all brain regions, are objects that lie on or inside a non-linear surface or manifold called the positive semidefinite cone. This non-Euclidean geometry of the FCs suggests that the distances between FCs are better measured along a geodesic of the cone. This is in contrast to using correlation which is equivalent to the cosine of the angle between demeaned and normalized FCs, or the Euclidean distance which is equivalent to the straight-line distance between FCs. Venkatesh and colleagues applied the geodesic method of comparison to the problem of participant identification and showed that it improves identification rates robustly compared to a dissimilarity measure based on correlation. The improvement was observed across most conditions (resting-state and 7 fMRI tasks) from the Human Connectome Project (HCP) dataset.

The definition of geodesic distance between two positive definite matrices of the same size (say  $Q_1$  and  $Q_2$ ) requires that at least one of the matrices being compared is invertible<sup>30</sup>. When this is not the case (rank deficient matrices with at least one eigenvalue equal to 0), one can regularize both  $Q_1$  and  $Q_2$  by adding a scaled identity matrix,  $\lambda * I$ , to both, which increases the eigenvalues of both matrices by  $\lambda$ , ensuring that they become invertible. For simplicity, this process was used by Venkatesh et al<sup>15</sup> with  $\lambda = 1$  when computing geodesic distances between rank deficient matrices. Rank deficient functional connectomes may occur typically when the number of time points (from the BOLD time-series) is smaller than the number of brain regions of the parcellation used. It may also happen when using high resolution parcellations. The authors demonstrated that even with rank-deficient matrices, with the help of regularization, participant identification rates increased when using geodesic distance.

Although  $\lambda = 1$  was used, in principle one could use any positive value of the regularization parameter,  $\lambda$ , and repeat the process of participant identification to assess performance. In addition, matrices which are already full rank and invertible may also benefit from the same regularization

procedure. In this technical note, we explore the effect of using different values of the regularization parameter ( $\lambda$ ) on the geodesic distance between FCs and its impact on participation identification rates. We assess this effect for different scanning lengths, parcellations and fMRI tasks and show that there is always an optimal  $\lambda$  which maximizes identification rates. In this manner, we develop a procedure to uncover functional fingerprints by shifting FC data to an optimal location of the semi-definite cone where FCs are more differentiable across participants.

## 2. Methods

### 2.1. Dataset

We included the  $N = 426$  unrelated subjects from the Human Connectome Project (HCP) 1200-participant release<sup>23</sup>. This subset of unrelated subjects was chosen from the overall dataset to ensure that no two subjects have a shared parent. The criterion to exclude siblings (whether they share one or both parents) was crucial to avoid confounding effects in our analyses due to family-structure confounders. Data from resting-state (REST) and seven fMRI tasks were used: emotion processing (EM), gambling (GAM), language (LAN), motor (MOT), relational processing (REL), social cognition (SOC) and working-memory (WM). In this study, we will refer to the resting-state plus all the tasks as *conditions*.

The resting-state fMRI scans were acquired on two different days, with two runs each with two different phase acquisitions – left to right or LR, and right to left or RL. Only the two runs from day one were used in this study. Like resting-state, each task had two runs (LR and RL), both of which were used in this study. The HCP scanning protocol was approved by the Institutional Review Board at Washington University in St. Louis. Full details on the HCP dataset have been published previously<sup>22,31,32</sup>.

### 2.2. Brain Parcellations

Two grey matter parcellations were used in this study:

- The **Destrieux** atlas<sup>33</sup>, or “aparc.2009s” in FreeSurfer nomenclature, defined using “Rules and algorithm that produced labels consistent with anatomical rules as well as automated computational parcellation,” featuring 75 regions in each hemisphere (74 + Medial Wall), with the particularity of separating gyral and sulcal areas (a total of 150 brain regions).
- **MMP1.0** atlas<sup>34</sup>, a multi-modal parcellation of the human cerebral cortex, with 180 brain regions in each hemisphere (a total of 360 brain regions).

For completeness, 14 subcortical regions were added to each parcellation, as provided by the HCP release (filename Atlas\_ROI2.nii.gz). To do so, this file was converted from NIFTI to CIFTI format using the HCP workbench software<sup>34,35</sup> (<http://www.humanconnectome.org/software/connectome-workbench.html>, command `-cifti-create-label`). This resulted in a total of 164 and 374 brain regions for Destrieux and MMP1.0 parcellations, respectively.

### 2.3. Preprocessing

The data processed using the ‘minimal’ preprocessing pipeline from the HCP was employed in this work<sup>31</sup>. This pipeline included artifact removal, motion correction, and registration to standard template. Full details on this pipeline can be found in earlier publications<sup>31,32</sup>.

We added the following steps to the ‘minimal’ processing pipeline. For resting-state fMRI data: (i) we regressed out the global gray-matter signal from the voxel time courses<sup>36</sup>, (ii) we applied a bandpass first-order Butterworth filter in the forward and reverse directions (0.001Hz to 0.08Hz<sup>36</sup>; Python function from the scipy package v1.2.1 *filtfilt*<sup>37,38</sup>), and (iii) the voxel time courses were z-scored and then averaged per brain region, excluding any outlier time points that were outside of 3 standard deviation from the mean (*workbench* software, command *-cifti-parcellate*). For task fMRI data, we applied the same steps as mentioned above but a more liberal frequency range was adopted for the band-pass filter (0.001Hz to 0.25Hz), since the relationship between different tasks and optimal frequency ranges is still unclear<sup>39</sup>.

Table 1 shows the number of frames per run for all conditions. It also shows the number of participants for whom this number of frames per run were available after the preprocessing. Any runs where we could not fully process the data or were left with fewer frames were left out of the analyses.

**Table 1**

Summary of the number of unrelated participants available (out of a total of 426) for each parcellation and condition after complete preprocessing of the fMRI data with corresponding number of frames per run.

condition	REST	EM	GAM	LAN	MOT	REL	SOC	WM
total participants – Destrieux	407	408	408	409	409	409	409	409
total participants – MMP1.0	405	406	406	407	407	407	407	407
frames per run	1190	166	243	306	274	222	264	395

### 2.4. Whole-brain Functional Connectomes

As described in Section 2.3, for a given brain parcellation, time series data for each voxel was z-scored and averaged within each brain region. Pearson’s correlation coefficient (MATLAB command *corr*) was used to estimate the functional connectivity between all pairs of brain regions, resulting in a symmetric correlation matrix of size  $m \times m$  where  $m$  is the number of brain regions in the parcellation being used. This object is referred to as a Functional Connectome (FC).

It is well known that correlation matrices are symmetric positive semi-definite (SPSD): their eigenvalues are greater than or equal to zero<sup>40</sup>. If all the eigenvalues of an FC are strictly greater

than zero, then it is a symmetric positive *definite* (SPD) matrix. The rank and invertibility of an FC are also directly related to its eigenvalues: if one or more eigenvalues are zero, then that FC is *rank-deficient* and not invertible. When all the eigenvalues are greater than zero for an FC, it is *full-rank* and hence invertible<sup>40</sup>. The rank of an FC depends on the number of brain regions in the parcellation and the number of samples in the time series such that:

$$\begin{aligned} \text{rank} &\leq m && \text{for } T \geq m \\ \text{rank} &< T && \text{for } T < m \end{aligned}$$

where  $m$  is the number of brain regions in the parcellation and  $T$  is the number of samples in the time series. For all the conditions, the FCs generated using Destrieux parcellation were full-rank if the number of samples (frames) in the time series was  $\geq 164$ , while the FCs generated using MMP1.0 parcellation were always rank-deficient, regardless of the number of samples in the time series (see Table 1).

An FC was computed for each of the two runs of each participant and each condition (resting-state and seven tasks).

## 2.5. Geometry of Functional Connectomes

Functional Connectomes (FCs) estimated using Pearson's correlation coefficient are objects that lie on or inside a non-linear surface, or manifold, called the positive semi-definite cone. Although a three-dimensional visualization of this manifold is only possible for 2x2 FCs (see Figure 1), a manifold with exactly the same properties exists for FCs with higher dimensions<sup>40</sup>. Pearson's correlation coefficient is the canonical way to estimate similarity/dissimilarity between FCs<sup>14,21</sup>, while other related approaches, such as Euclidean distance between the vectorized matrices<sup>41</sup> and the so called Manhattan ( $L^1$ ) distance<sup>42</sup>, have also been used. Considering the non-Euclidean geometry of FCs, it is natural to measure the distance between FCs along the curvature of the positive semi-definite cone<sup>40</sup>. The geodesic distance between two points inside the cone, thus between two SPD FCs  $Q_1$  and  $Q_2$ , is the shortest path between them along the manifold and is unique for any two such points<sup>30,40</sup>.

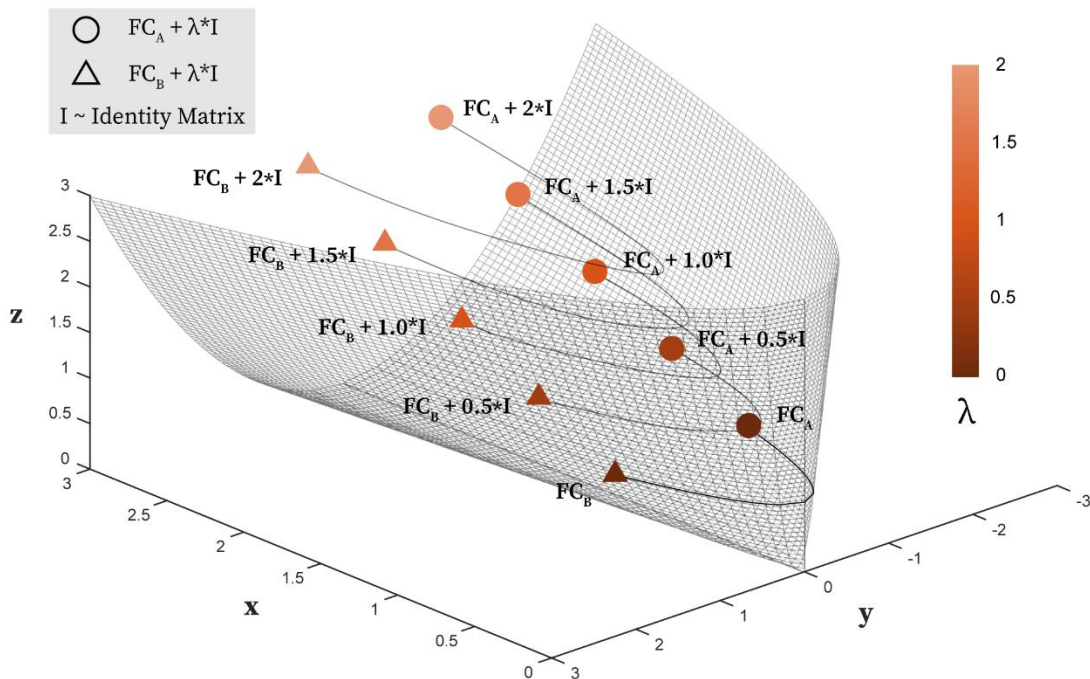
Let  $\mathbb{S}_+^M$  be the set of all symmetric positive matrices of dimension  $M$ , which lie on or inside a symmetric positive semi-definite cone of dimension  $M$ . The positive-definite matrices would comprise the interior of the cone while all the rank-deficient semi-definite matrices would reside on the cone boundary. Now assume that  $Q_1 \in \mathbb{S}_+^m$  and  $Q_2 \in \mathbb{S}_+^m$  are two SPD matrices of size  $m \times m$  (here,  $m = 164$  or  $374$ ). Let us denote  $Q = Q_1^{-\frac{1}{2}} Q_2 Q_1^{-\frac{1}{2}}$ , then  $Q \in \mathbb{S}_+^m$  and its corresponding  $m$  eigenvalues satisfy  $\lambda_i^Q \geq 0$  ( $1 \leq i \leq m$ ). Then the geodesic distance between  $Q_1$  and  $Q_2$  is computed as<sup>30,40</sup>:

$$d_G(Q_1, Q_2) = \sqrt{\text{trace} \left( \log^2 \left( Q_1^{-\frac{1}{2}} Q_2 Q_1^{-\frac{1}{2}} \right) \right)} = \sqrt{\text{trace}(\log^2(Q))} = \sqrt{\sum_{i=1}^m (\log(\lambda_i^Q))^2}$$

where  $\log$  is the matrix log operator. This definition of geodesic distance requires that the matrix  $Q_1$  is invertible (or equivalently SPD or full-rank). When this is not the case, we can regularize both  $Q_1$  and  $Q_2$  by adding to each of them a scaled identity matrix,  $\lambda * I$ , which increases the value of their eigenvalues by  $\lambda$ , ensuring that they are now invertible matrices. Importantly, this regularization reallocates both matrices within the positive semi-definite cone (Figure 1). Venkatesh et al.<sup>15</sup> used this regularization process and got significantly higher participant identification rates based on geodesic distance than the ones achieved with Pearson's correlation.

Venkatesh et al.<sup>15</sup> used  $\lambda = 1$  with the specific purpose of ensuring full rank matrices. However, theoretically, one could use any positive value of the regularization parameter,  $\lambda$ , to ensure that both matrices ( $Q_1$  and  $Q_2$ ) are full-rank. As mentioned earlier, all correlation matrices are either positive definite or positive semi-definite, which means that either all their eigenvalues are positive or at least one of them is zero (they cannot have negative eigenvalues). Thus, even a small positive perturbation to a rank-deficient correlation matrix using a scaled identity matrix would make it full-rank and invertible (i.e. all eigenvalues greater than zero).

### Geometry-aware visualization of Geodesic distance and effect of regularization



A generic 2x2 FC matrix:

$$\begin{bmatrix} x & y \\ y & z \end{bmatrix}$$

Since FC matrices are symmetric and positive semi-definite, they satisfy the conditions:

$$\begin{aligned} x &\geq 0 \\ z &\geq 0 \\ xz - y^2 &\geq 0 \end{aligned}$$

**Figure 1. Incremental regularization of functional connectomes (FCs) and its effect on the estimates of geodesic distance.** We illustrate the geodesic distance between two FCs of size 2x2 (denoted here by a circle and a triangle) and how it changes with increasing regularization ( $\lambda$ ) of FCs. All the positive-definite (full rank) FCs comprise the cone interior while all the rank-deficient positive semi-definite FCs (having at least one 0 eigenvalue) reside on the cone boundary. Different magnitudes of  $\lambda$  reallocate FCs within the positive semi-definite cone. We should also highlight that for FCs of higher dimensions, a three-dimensional visualization of the positive semi-definite cone is not possible.

## 2.6. Participant Identification

Participant identification is the process of identifying an individual's FC from a population of FCs, given another FC of that individual. All conditions (resting-state and seven tasks) in our dataset contain 2 runs (LR and RL acquisition orientation), which we denominate here Test and Retest. In order to avoid any bias due to the acquisition orientation, runs were randomly assigned to either Test or Retest for each subject. This process was repeated for each condition separately.

An FC from the Retest data was labeled with the participant's identity in the Test data that was closest to it in the Test data. We repeated this process for all the FCs in the Retest data and defined the identification rate as:

$$\text{Identification Rate} = \frac{\text{Number of correctly labeled participants}}{\text{Total number of participants}}$$

The identification rates were computed for each condition separately. To study the effects of regularization on the identification rates, this process was repeated for a wide range of regularization parameter values,  $\lambda$ , in particular:

$$\text{For Destrieux parcellation: } \lambda = \begin{cases} \langle 0 \rangle \text{ to } \langle 2 \rangle \text{ in steps of } 0.1 \\ \langle 2.5 \rangle \text{ to } \langle 10 \rangle \text{ in steps of } 0.5 \end{cases}$$

$$\text{For MMP1.0 parcellation: } \lambda = \begin{cases} \langle 0 \rangle \text{ to } \langle 10 \rangle \text{ in steps of } 0.5 \\ \langle 11 \rangle \text{ to } \langle 20 \rangle \text{ in steps of } 1 \end{cases}$$

To understand the effect of scanning length (or the number of frames), for each value of  $\lambda$ , the identification process was repeated for different number of frames (samples) in the time series. For both parcellations, effect of scanning length was assessed starting from 50 frames to the maximum number of frames, in steps of 50 (see Table 1 for maximum number of available frames for all conditions).

To assess variability in identification performance due to differences in samples, we used sampling without replacement. For every run, we randomly selected 70% of the participants and performed participant identification. This procedure was repeated 100,000 times for each value of  $\lambda$  and for each number of frames evaluated.

### 3. Results

In this technical note we explored the effect of using different values of the regularization parameter ( $\lambda$ ) on the geodesic distance, which was recently used by Venkatesh et al.<sup>15</sup> to compare FCs. We studied how this variable regularization affects participant identification rates for FCs, with different conditions (resting-state and seven fMRI tasks), parcellations and varying scanning length.

Participant identification rates for all conditions and different parcellations appeared to be a roughly convex function of  $\lambda$ . In most cases, we observed the presence of an optimal  $\lambda$  value for which the identification rate is maximum. For a few cases, it seems that there is a range of optimal  $\lambda$ s that produce very similar identification rates.

Using the maximum available number of frames, the optimal value of  $\lambda$ , that maximized the identification rate depended not only on the condition but also on the parcellation (Figure 2). For each condition, we observed an optimal value or range of values of  $\lambda$ s that maximized the identification rates. The optimal values of  $\lambda$  was smaller for the Destrieux parcellation than for the MMP1.0 parcellation for any given condition. Resting-state, language and working-memory had the highest, while the emotion task had the lowest identification rates at the optimal points for both parcellations. At the optimal points, the identification rates were either approximately equal (for resting-state) or better when using MMP1.0 parcellation, compared to Destrieux, except for working-memory and social tasks. For both parcellations, resting-state condition reached greater than 99% identification rate at the optimal point.

With the Destrieux parcellation (164 brain regions), in general, the optimal value of  $\lambda$  was very small (0.1–0.2) for resting-state compared to tasks, with identification rates decreasing slowly with increasing magnitudes (see Figure 3). Overall, for resting-state compared to tasks, the number of frames used to compute FCs played a much bigger role in participant identification rates than the regularization magnitude. For a given  $\lambda$ , the identification rates tended to increase with increasing number of frames for all conditions. With fewer number of frames, a broader range of  $\lambda$  optimized the identification rates. But as the number of frames increased, this range became narrower and hence maximal identification rates required more specific regularization. Also, the drop off in identification rates was sharper when the optimal  $\lambda$  range became more narrow. This pattern is less clear with the emotion task, perhaps due to the availability of fewer time frames than in other tasks (see Table 1).

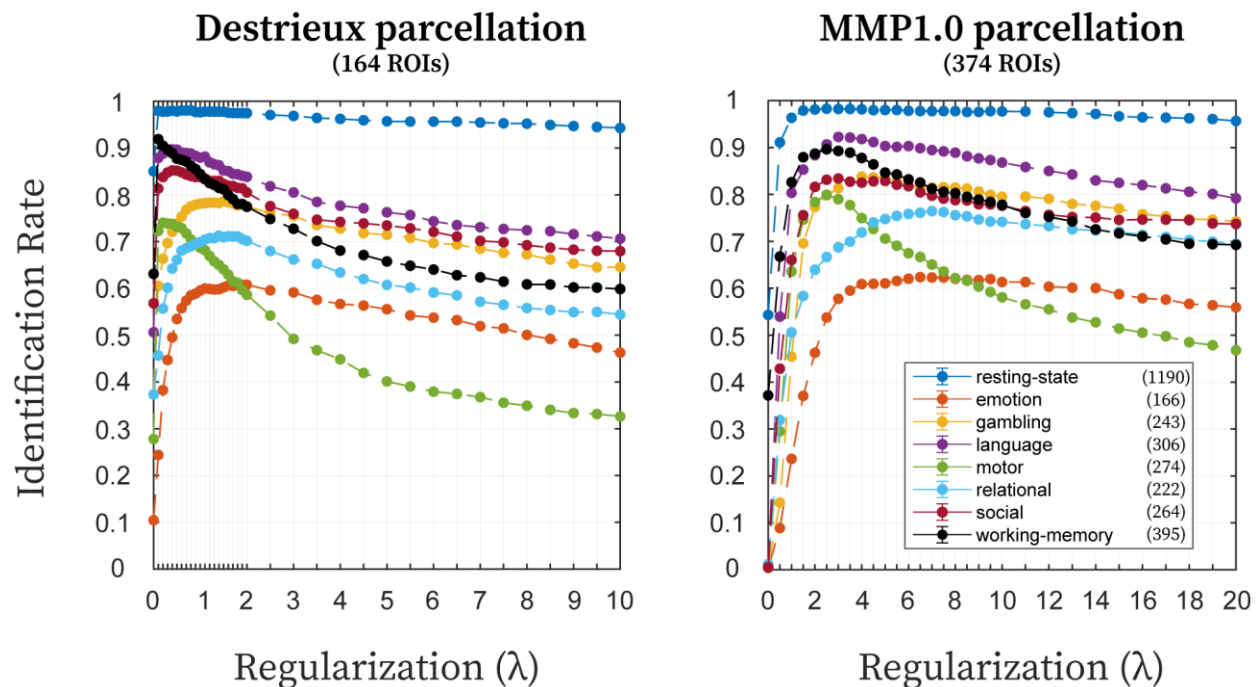


**Figure 2: Effect of regularization ( $\lambda$ ) on participant identification rates.** Participant identification rates for all eight conditions (utilizing maximum available frames) with variable magnitudes of  $\lambda$ , using Destrieux (left; 164 ROIs) and MMP1.0 (right; 374 ROIs) parcellations. Error bars indicate the standard error of the mean across cross-validation resamples (error bars are small enough that they are hidden behind the dots). Legend indicates the eight conditions along with maximum available number of frames.

With MMP1.0 parcellation (374 brain regions), we observed similar results. Just as with the Destrieux parcellation, resting-state behaved differently than tasks. First, for any given number of frames, the optimal values of  $\lambda$  were much smaller for resting-state than tasks (Figure 4). Second, the identification rates for resting-state were dependent more on the number of frames than on the regularization. For a given  $\lambda$ , the identification rates tended to increase with increasing number of frames for all conditions. Finally, the optimal ranges of  $\lambda$ s were broader with fewer number of frames and narrowed with increasing number of frames. In comparison to the Destrieux parcellation, the narrowing of the optimal  $\lambda$  range required greater number of frames for MMP1.0 for any given condition.

### Participation Identification Rates for Destrieux parcellation

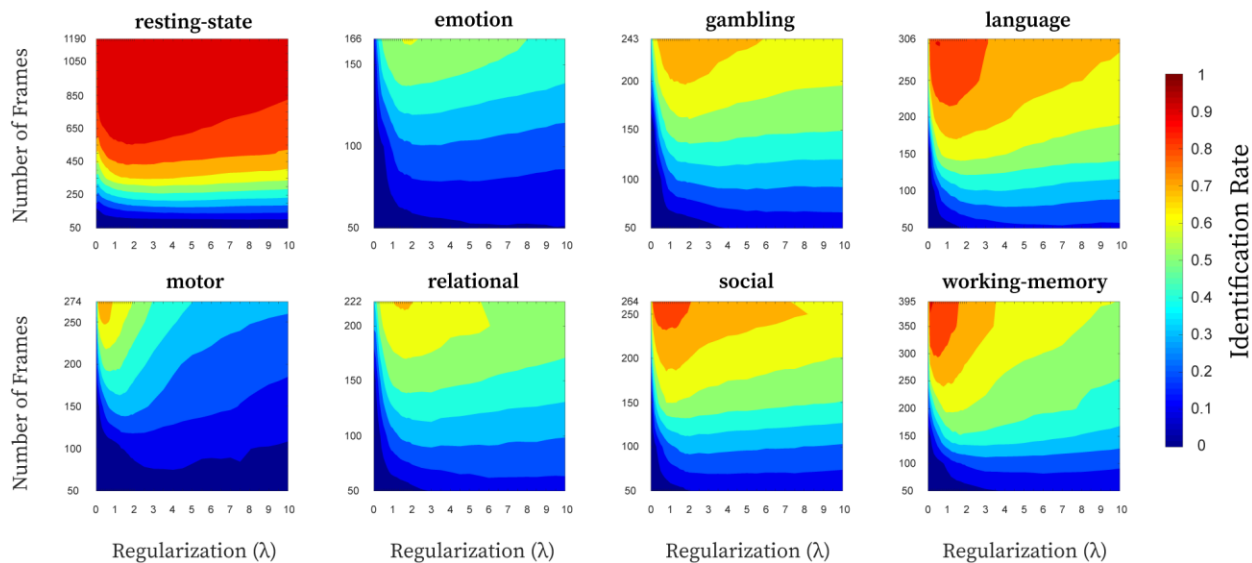


**Figure 3: Participant identification rates as a function of regularization ( $\lambda$ ) and the number of frames used to compute FCs using Destrieux parcellation.** The panel shows identification rates for all eight conditions. For any given condition, the frames were selected *sequentially* out of the total time series ranging from 50 to maximum number of frames available, in steps of 50.

## Participation Identification Rates for **MMP1.0** parcellation

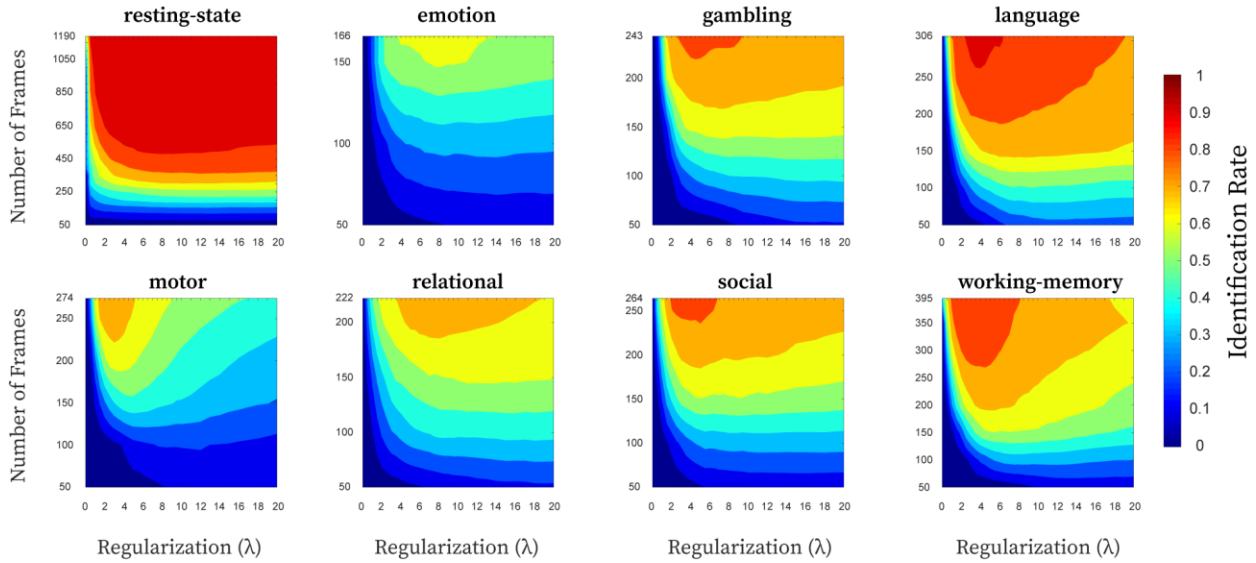


**Figure 4: Participant identification rates as a function of regularization ( $\Lambda$ ;  $\lambda$ ) and the number of frames used to compute FCs using MMP1.0 parcellation.** The panel shows identification rates for all eight conditions. For any given condition, the frames were selected *sequentially* out of the total time series ranging from 50 to maximum number of frames available, in steps of 50.

## 4. Discussion

In this work, we explored the effects of different magnitudes of regularization on geodesic distance and subsequently its impact on participant identification rates in Functional Connectomes (FCs). We explored these effects for eight fMRI conditions from the HCP data — resting-state, emotion, gambling, language, motor, relational, social and working-memory. We found that the optimal value of the regularization parameter, which maximized the participant identification rates, is dependent on the condition, parcellation and the number of frames used to compute the FCs. In addition, the deviation from the optimal point could affect the identification rates drastically depending on the condition and the number of frames used. In short, we found that geodesic distance, which has been shown to be a more accurate way of comparing FCs than canonical methods<sup>15</sup>, can be further improved by choosing an optimal regularization magnitude for each dataset and fMRI condition.

### 4.1. Identification rate is a roughly convex function of the regularization parameter

We observed that for any condition and parcellation, there was a specific value or a range of values for the regularization parameter where the identification rate maximized i.e. the identification rate was a convex function of the regularization parameter. We should emphasize that only a limited range of the regularization parameter was tested in this study, for specific conditions and parcellations, and thus we cannot guarantee that this phenomenon would generalize to other datasets. But, considering the breadth of the fMRI conditions and the size of the dataset used in this study, we are confident this behavior would be replicable in other datasets as well.

#### ***4.2. Optimal regularization parameter depends on the specific dataset***

We observed that the optimal value of the regularization parameter, which maximizes the identification rates, depends on the condition, parcellation and number of frames used to compute the FCs. Venkatesh et al.<sup>15</sup> used a fixed regularization magnitude ( $\lambda = 1$ ). Here we show that identification rates can be substantially improved by using dataset-dependent regularization parameter. In addition, although Venkatesh et al.<sup>15</sup> employed regularization only when the FCs being compared were rank-deficient, we found that regularization improves identification rates even with full-rank FCs; this was the case of Destrieux parcellation when  $\geq 164$  frames were used to compute FCs.

#### ***4.3. Longer scanning length leads to more specific values of optimal regularization***

As the number of samples (or frames) increase in the time series data, the resultant correlations become more reliable<sup>43</sup> and thus we get better estimates of the FCs. For all the tasks, we observed that as the number of frames increased, the range of values of  $\lambda$  which resulted in maximized identification rates narrowed. This effect was not as prominent in resting-state, where for most of the number of frames evaluated, there was a wide range of values of  $\lambda$  which resulted in maximum identification rates. This suggests that resting-state FCs, in comparison to tasks, may reside in an intrinsically different region of the semi-definite cone where reallocation of FCs through regularization does not have a sizeable influence on their differentiability.

#### ***4.4. Regularization helps compensate for a coarser grain parcellation***

Using Pearson's correlation as a similarity metric to compare FCs, Finn et al.<sup>14</sup> showed that a parcellation with more ROIs resulted in higher participant identification rates than a parcellation with fewer ROIs. Venkatesh et al.<sup>15</sup> observed the same trend with both geodesic distance and Pearson's correlation-based dissimilarity. This suggested that finer parcellations lead to more uniqueness or fingerprint, at least up to a certain resolution. In this work, we found that when using a coarser resolution parcellation, we can achieve similar and sometimes even better identification rates than a finer resolution parcellation when applying geodesic distance with optimal regularization magnitude.

#### ***4.4. How to estimate the regularization parameter in different studies***

We have observed that the optimal regularization that leads to maximum identification rates is dependent on the fMRI condition, brain parcellation and scanning length. There might be other aspects of the data that influence such optimal value as well, such as voxel size or repetition time. Hence, results suggest that when using geodesic to compare FCs, the regularization parameter must be estimated from the FC data of that study. Also, one should utilize sampling techniques to estimate a mean or median magnitude of regularization, along with the corresponding error. Once an appropriate magnitude has been identified, one should regularize all FCs in the dataset by that amount, and then use geodesic distance to compare FCs.

## **5. Conclusion**

The use of the geodesic distance on full-rank or regularized rank-deficient FCs, has been shown to be a more principled and accurate method to compare FCs than canonical methods, ultimately leading to improved subject fingerprinting, as measured by identification rates. Here we show that the approach can be further improved by finding an optimal value of regularization for FCs that uncovers brain connectivity fingerprints by means of an incremental assessment of the magnitude of the regularization parameter. We show that optimal regularization that maximizes participant identification rates is highly dataset-dependent — it depends on the fMRI condition, on the brain parcellation used, and on the number of frames used to compute the FCs.

## **ACKNOWLEDGMENTS**

Data were provided [in part] by the Human Connectome Project, WU-Minn Consortium (Principal Investigators: David Van Essen and Kamil Ugurbil; 1U54MH091657) funded by the 16 NIH Institutes and Centers that support the NIH Blueprint for Neuroscience Research; and by the McDonnell Center for Systems Neuroscience at Washington University.

## **FUNDING INFORMATION**

JG acknowledges financial support from NIH R01EB022574, NIH R01MH108467, Indiana Alcohol Research Center P60AA07611, and Purdue Discovery Park Data Science Award "Fingerprints of the Human Brain: A Data Science Perspective". JH has been partially supported by the grant NIH R01MH108467.

## Bibliography

1. Ogawa S, Lee TM, Kay AR, Tank DW. Brain magnetic resonance imaging with contrast dependent on blood oxygenation. *Proc Natl Acad Sci U S A*. 1990. doi:10.1073/pnas.87.24.9868
2. Ogawa S, Tank DW, Menon R, et al. Intrinsic signal changes accompanying sensory stimulation: Functional brain mapping with magnetic resonance imaging. *Proc Natl Acad Sci U S A*. 1992. doi:10.1073/pnas.89.13.5951
3. Kwong KK, Belliveau JW, Chesler DA, et al. Dynamic magnetic resonance imaging of human brain activity during primary sensory stimulation. *Proc Natl Acad Sci U S A*. 1992. doi:10.1073/pnas.89.12.5675
4. Bandettini PA, Wong EC, Hinks RS, Tikofsky RS, Hyde JS. Time course EPI of human brain function during task activation. *Magn Reson Med*. 1992. doi:10.1002/mrm.1910250220
5. Frahm J, Bruhn H, Merboldt K -D, Hänicke W. Dynamic MR imaging of human brain oxygenation during rest and photic stimulation. *J Magn Reson Imaging*. 1992. doi:10.1002/jmri.1880020505
6. Galton F. Regression Towards Mediocrity in Hereditary Stature. *J Anthropol Inst Gt Britain Irel*. 1886. doi:10.2307/2841583
7. Bravais A. *Analyse Mathématique Sur Les Probabilités Des Erreurs de Situation d'un Point*. Impr. Royale; 1844.
8. Zuo XN, He Y, Betzel RF, Colcombe S, Sporns O, Milham MP. Human Connectomics across the Life Span. *Trends Cogn Sci*. 2017. doi:10.1016/j.tics.2016.10.005
9. Shen X, Finn ES, Scheinost D, et al. Using connectome-based predictive modeling to predict individual behavior from brain connectivity. *Nat Protoc*. 2017. doi:10.1038/nprot.2016.178
10. Svaldi DO, Goñi J, Abbas K, et al. Optimizing Differential Identifiability Improves Connectome Predictive Modeling of Cognitive Deficits in Alzheimer's Disease. *arXiv Prepr arXiv190806197*. 2019.
11. Fornito A, Zalesky A, Breakspear M. The connectomics of brain disorders. *Nat Rev Neurosci*. 2015;16(3):159-172. doi:10.1038/nrn3901
12. Fornito A, Bullmore ET. Connectomics: A new paradigm for understanding brain disease. *Eur Neuropsychopharmacol*. 2015. doi:10.1016/j.euroneuro.2014.02.011
13. van den Heuvel MP, Sporns O. A cross-disorder connectome landscape of brain dysconnectivity. *Nat Rev Neurosci*. 2019. doi:10.1038/s41583-019-0177-6
14. Finn ES, Shen X, Scheinost D, et al. Functional connectome fingerprinting: Identifying individuals using patterns of brain connectivity. *Nat Neurosci*. 2015. doi:10.1038/nn.4135
15. Venkatesh M, Jaja J, Pessoa L. Comparing functional connectivity matrices: A geometry-aware approach applied to participant identification. *Neuroimage*. November 2019:116398. doi:10.1016/J.NEUROIMAGE.2019.116398
16. Seitzman BA, Gratton C, Laumann TO, et al. Trait-like variants in human functional brain networks. *Proc Natl Acad Sci U S A*. 2019;116(45):22851-22861. doi:10.1073/pnas.1902932116

17. Mars RB, Passingham RE, Jbabdi S. Connectivity Fingerprints: From Areal Descriptions to Abstract Spaces. *Trends Cogn Sci*. 2018. doi:10.1016/j.tics.2018.08.009
18. Satterthwaite TD, Xia CH, Bassett DS. Personalized Neuroscience: Common and Individual-Specific Features in Functional Brain Networks. *Neuron*. 2018;98(2):243-245. doi:10.1016/j.neuron.2018.04.007
19. Gratton C, Laumann TO, Nielsen AN, et al. Functional Brain Networks Are Dominated by Stable Group and Individual Factors, Not Cognitive or Daily Variation. *Neuron*. 2018. doi:10.1016/j.neuron.2018.03.035
20. Pallarés V, Insabato A, Sanjuán A, et al. Extracting orthogonal subject- and condition-specific signatures from fMRI data using whole-brain effective connectivity. *Neuroimage*. 2018;178:238-254. doi:10.1016/j.neuroimage.2018.04.070
21. Amico E, Goñi J. The quest for identifiability in human functional connectomes. *Sci Rep*. 2018. doi:10.1038/s41598-018-25089-1
22. Van Essen DC, Ugurbil K, Auerbach E, et al. The Human Connectome Project: A data acquisition perspective. *Neuroimage*. 2012;62(4):2222-2231. doi:10.1016/j.neuroimage.2012.02.018
23. Van Essen DC, Smith SM, Barch DM, Behrens TEJ, Yacoub E, Ugurbil K. The WU-Minn Human Connectome Project: An overview. *Neuroimage*. 2013. doi:10.1016/j.neuroimage.2013.05.041
24. Amunts K, Ebell C, Muller J, Telefont M, Knoll A, Lippert T. The Human Brain Project: Creating a European Research Infrastructure to Decode the Human Brain. *Neuron*. 2016. doi:10.1016/j.neuron.2016.10.046
25. Allen NE, Sudlow C, Peakman T, Collins R. UK biobank data: Come and get it. *Sci Transl Med*. 2014. doi:10.1126/scitranslmed.3008601
26. Miller KL, Alfaro-Almagro F, Bangerter NK, et al. Multimodal population brain imaging in the UK Biobank prospective epidemiological study. *Nat Neurosci*. 2016. doi:10.1038/nn.4393
27. Okano H, Miyawak A, Kasai K. Brain/MINDS: Brain-mapping project in Japan. *Philos Trans R Soc B Biol Sci*. 2015. doi:10.1098/rstb.2014.0310
28. Poo M ming, Du J lin, Ip NY, Xiong ZQ, Xu B, Tan T. China Brain Project: Basic Neuroscience, Brain Diseases, and Brain-Inspired Computing. *Neuron*. 2016. doi:10.1016/j.neuron.2016.10.050
29. Bari S, Amico E, Vike N, Talavage TM, Goñi J. Uncovering multi-site identifiability based on resting-state functional connectomes. *Neuroimage*. 2019. doi:10.1016/j.neuroimage.2019.06.045
30. Pennec X, Fillard P, Ayache N. A riemannian framework for tensor computing. *Int J Comput Vis*. 2006. doi:10.1007/s11263-005-3222-z
31. Glasser MF, Sotiropoulos SN, Wilson JA, et al. The minimal preprocessing pipelines for the Human Connectome Project. *Neuroimage*. 2013. doi:10.1016/j.neuroimage.2013.04.127
32. Smith SM, Beckmann CF, Andersson J, et al. Resting-state fMRI in the Human Connectome Project. *Neuroimage*. 2013. doi:10.1016/j.neuroimage.2013.05.039
33. Destrieux C, Fischl B, Dale A, Halgren E. Automatic parcellation of human cortical gyri and sulci using standard anatomical nomenclature. *Neuroimage*. 2010.

doi:10.1016/j.neuroimage.2010.06.010

34. Glasser MF, Coalson TS, Robinson EC, et al. A multi-modal parcellation of human cerebral cortex. *Nature*. 2016. doi:10.1038/nature18933
35. Marcus DS, Harwell J, Olsen T, et al. Informatics and data mining tools and strategies for the human connectome project. *Front Neuroinform*. 2011. doi:10.3389/fninf.2011.00004
36. Power JD, Mitra A, Laumann TO, Snyder AZ, Schlaggar BL, Petersen SE. Methods to detect, characterize, and remove motion artifact in resting state fMRI. *Neuroimage*. 2014. doi:10.1016/j.neuroimage.2013.08.048
37. Gustafsson F. Determining the initial states in forward-backward filtering. *IEEE Trans Signal Process*. 1996. doi:10.1109/78.492552
38. Virtanen P, Gommers R, Oliphant TE, et al. SciPy 1.0: fundamental algorithms for scientific computing in Python. *Nat Methods*. 2020. doi:10.1038/s41592-019-0686-2
39. Cole MW, Bassett DS, Power JD, Braver TS, Petersen SE. Intrinsic and task-evoked network architectures of the human brain. *Neuron*. 2014. doi:10.1016/j.neuron.2014.05.014
40. Bhatia R. *Positive Definite Matrices*.; 2009. doi:10.2307/2317709
41. Ponsoda V, Martínez K, Pineda-Pardo JA, et al. Structural brain connectivity and cognitive ability differences: A multivariate distance matrix regression analysis. *Hum Brain Mapp*. 2017. doi:10.1002/hbm.23419
42. Allen EA, Damaraju E, Plis SM, Erhardt EB, Eichele T, Calhoun VD. Tracking whole-brain connectivity dynamics in the resting state. *Cereb Cortex*. 2014. doi:10.1093/cercor/bhs352
43. Bonett DG, Wright TA. Sample size requirements for estimating Pearson, Kendall and Spearman correlations. *Psychometrika*. 2000. doi:10.1007/BF02294183